Translational Oncology 14 (2021) 101018

Contents lists available at ScienceDirect

Translational Oncology

journal homepage: www.elsevier.com/locate/tranon

Original Research

Absent in melanoma 2-mediating M1 macrophages facilitate tumor rejection in renal carcinoma

Dafei Chai[a,b,*], Zichun Zhang[a,c], Shang yuchen Shi[d], Dong Qiu[c], Chen Zhang[a], Gang Wang[a,b], Lin Fang[a,b], Huizhong Li[a,b], Hui Tian[a,b], Hailong Li[c], Junnian Zheng[a,b,*]

[a] Cancer Institute, Xuzhou Medical University, Xuzhou, Jiangsu 221002, P.R. China
[b] Center of Clinical Oncology, Affiliated Hospital of Xuzhou Medical University, Xuzhou Medical University, Xuzhou, Jiangsu 221002, P.R. China
[c] Department of Urology, Affiliated Hospital of Xuzhou Medical University, Xuzhou, Jiangsu 221002, P.R. China
[d] Department of Radiation Oncology, Affiliated Hospital of Xuzhou Medical University, Xuzhou, Jiangsu 221002, P.R. China

ARTICLE INFO

Keywords:
Renal carcinoma
TAMs
Macrophage polarization
AIM2
Inflammasome

ABSTRACT

Absent in melanoma 2 (AIM2) as an immune regulator for the regulation of tumor-associated macrophages (TAMs) function is unclear in tumor development. Here, the AIM2 function was investigated in TAMs-mediated malignant behaviors of renal carcinoma. The correlation analysis result showed that the AIM2 expression in TAMs was negatively correlated with the percentages of M2-like polarization phenotype in human or murine renal cancer specimens. By the cocultured assay with bone marrow-derived macrophages (BMDMs) and Renca cells, overexpression of AIM2 in macrophages enhanced the inflammasome activation and reversed the phenotype from M2 to M1. Compared with BMDMs-Ctrl cocultured group, BMDMs-AIM2 cocultured group showed reduced tumor cell proliferation and migration. The blockade of inflammasome activation by the inhibitor Ac-YVAD-CMK abrogated AIM2-mediated M1 polarization and the inhibition of tumor cell growth. To evaluate the therapeutic efficacy of AIM2-mediated M1 macrophages in vivo, BMDMs-AIM2 were intravenously injected into subcutaneous Renca-tumor mice. The results showed that the infiltration of M1 TAMs was increased and tumor growth was suppressed in BMDMs-AIM2-treated mice when compared with BMDMs-Ctrl-treat mice. Accordingly, the blockade of inflammasome activation reduced the anti-tumor activities of BMDMs-AIM2. Moreover, the lung metastases of renal carcinoma were suppressed by the administration of BMDMs-AIM2 accompanied with the reduced tumor foci. These results demonstrated that AIM2 enhanced TAMs polarization switch from anti-inflammatory M2 phenotypy to pro-inflammatory M1 through inflammasome signaling activation, thus exerting therapeutic intervention in renal carcinoma models. Our results provide a possible molecular mechanism for the modulation of TAMs polarization in tumor microenvironment and open a new potential therapeutic approach for renal cancer.

Introduction

Among urinary system tumors, renal carcinoma is the most common and lethal tumor [1]. The epidemiology indicates that renal carcinoma accounts for about 3% of all the mortality of human malignant tumors and grows increasingly every year [2–4]. Renal carcinoma represents a poor prognosis, because most patients have been already examined distal metastases at the initial diagnosis or after treatment by primary tumor resection [5,6]. Nowadays, the development of therapies aimed at tumor signaling pathways or immunotherapies have improved the treatment of metastasis renal carcinoma, but there is less effective treatment available [7,8]. Therefore, new therapeutic approaches urgently need to be developed for renal carcinoma.

Renal carcinoma is an immunogenic tumor and represents an immunosuppression in patients, and its growth and metastasis is linked to the impaired anti-tumor immunity [9]. Tumor-associated macrophages (TAMs) as the important immunosuppression cells are crucial for tumor growth, progression, and metastasis in a tumor microenvironment, and also are associated with poor prognosis in several human cancers [10,11]. Macrophages display a high plasticity, which allows them to adapt to their phenotype in response to different environmental stimuli [12,13]. TAMs exist in two different states of polarization classified as M1-like activated phenotype and an alternatively M2-like activated phenotype. M1 macrophages are characterized by the expression of pro-inflammatory cytokines (such as TNF-α, IL-1β, IL-6, and IL-12) and inducible nitric oxide synthase (iNOS) and show a protective role in tumor

* Corresponding author at: Cancer Institute, Xuzhou Medical University, 84 West Huaihai Road, Xuzhou, Jiangsu 221002, China.
E-mail addresses: chaidafei@xzhmu.edu.cn (D. Chai), jnzheng@xzhmu.edu.cn (J. Zheng).

https://doi.org/10.1016/j.tranon.2021.101018
Received 4 November 2020; Received in revised form 6 January 2021; Accepted 11 January 2021

genesis by activating tumor-killing mechanisms [14]. The alternatively activated M2 macrophages produce anti-inflammatory factors (like IL-10 and the mannose receptor CD206), which are clearly involved in immune suppression by promoting tumor growth, invasion, and metastases [15]. TAMs differentiation and polarization by distinct mechanisms are influenced by cancer processes, tumor microenvironment, and responsiveness to stimuli [16]. However, the molecular mechanisms that underlie TAMs polarization in renal carcinoma remain largely debated. Therefore, it is valuable to investigate the mechanism of TAMs-mediated tumor cell immune escape, which facilitates to find the effective approaches for renal carcinoma treatment.

Absent in melanoma 2 (AIM2) is a cytoplasmic DNA senor and belongs to an IFN-inducible PYHIN proteins family (pyrin and HIN200 domain-containing proteins). AIM2 binds to double-stranded DNA (dsDNA) and engages the inflammasome assembly by recruiting the adaptor protein apoptosis-associated speck-like protein containing a caspase-recruitment domain (ASC). The inflammasome-mediating caspase-1 activation results in the cleavage of pro-IL-1β and pro-IL-18 to trigger the maturation of pro-inflammatory cytokines IL-1β [17–19]. AIM2 inflammasome as a critical regulator of immune responses has been identified to play an important role in immune cell-mediated inflammatory diseases in recent years [20,21]. The previous study has reported that AIM2 promotes macrophage functional maturation in lupus nephritis [22]. Moreover, AIM2 contributes to autoimmune disorders in the autoimmune model [23,24]. AIM2 as a tumor regulator is involved in cancer cell migration, invasion, and tumor progression [25]. The overexpression of AIM2 inhibits cancer cell proliferation in colon cancer, breast cancer, prostate cancer, or renal cancer [26–29]. Thus, these results suggest that AIM2 plays an important role in the development and progression of inflammatory diseases.

Yet, the multiple roles of AIM2 have been studied in infection, cancer, and autoimmunity [30], the function of AIM2 in TAMs differentiation during the tumor microenvironment of renal carcinoma remains poorly understood. In this study, we explored the hypothesis whether AIM2 could inhibit the development of renal carcinoma through the reversal of TAMs differentiation. The results indicated that AIM2 expression in TAMs was negatively correlated with the percentages of M2-like TAMs. The overexpression of AIM2 reversed renal carcinoma cell-induced macrophage phenotype M2 transfer to M1. AIM2-mediated M1 could inhibit the malignant behaviors of renal carcinoma cells through the inflammasome activation pathway, and also suppressed the tumor growth in the primary tumor model or lung metastasis model. Our results revealed the possible molecular mechanism for the modulation of TAMs differentiation, which involved the pathogenesis of renal cancer. AIM2-mediated M1 might represent a novel therapeutic approach for renal cancer treatment.

Materials and methods

Human specimens and mice

Tumor tissue specimens of renal cancer patients ($n = 15$) who accepted curative surgery without prior treatment at the Department of Pathology of the Affiliated Hospital of Xuzhou Medical University from 2017 to 2019 were enrolled in this study. The corresponding paracarcinoma tissues were as the control. This study was performed under a protocol approved by the Institutional Review Boards of the Affiliated Hospital of Xuzhou Medical University. All examinations involving human subjects were performed after obtaining informed patient consent.

Female BALB/c mice 6- to 8-weeks of age were obtained from Vital River Laboratory Animal Technology Co., Ltd (Beijing, China) and housed in a specific pathogen-free room under controlled temperature and humidity. Animal care and all experimental procedures were performed in strict accordance with the Guide for the Care and Use of Medical Laboratory Animals. Animal care and all experimental procedures approved by the guidelines of the Laboratory Animal Ethical Committee of Xuzhou Medical University.

Preparation of single-cell suspension

To prepare single-cell suspensions, specimen tissues were dissected into smaller pieces and digested before being homogenized through 200-gage mesh cell strainers to generate single-cell suspensions. The cells were collected and then centrifuged at 750 g for 5 min. After centrifugation, the supernatant was discarded and the pellet of cells was washed with phosphate buffered saline (PBS). Red blood cells were lysed with the ACK lysis buffer.

Real-time PCR

Total RNA were extracted from collected samples by Trizol (Invitrogen, Eugene, OR, USA) and reverse-transcribed using a cDNA synthesis kit (TaKaRa) according to the manufacturer's instructions. The expression of the genes encoding GAPDH, AIM2, iNOS, CD206, Arg-1, IL-10, IL-12, and TNF-α was quantified by real-time PCR using 7900HT qPCR system thermal cycler (Applied Biosystems) and SYBR Green system (Takara Diagnostic Systems) normalized by the GAPDH expression following the manufacturer's protocol. The used primers were presented in Table 1.

Cell culture

HEK293T and L929 cells were obtained from ATCC; Renca cells were purchased from Cobioer Biosciences. These cells were cultured in DMEM or RPMI1640 medium containing 10% fetal bovine serum (FBS, HyClone), 100 U/mL penicillin, and 100 μg/mL streptomycin at 37 °C and 5% CO2. Renca cells were cultured in RPMI1640 medium supplemented with 10% FBS, 100 U/mL penicillin and 100 μg/mL streptomycin, 2 mM L-glutamine (Sigma), 0.1 mM non-essential amino acid (Sigma), and 1 mM sodium pyruvate (Sigma) in 5% CO2 atmosphere at 37 °C. All cells were authenticated by short tandem repeat profiling or certificate of analysis, and passaged for less than 6 weeks before renewal from frozen, early-passage stocks. All experiments were performed with mycoplasma-free cells.

Induction of BMDMs

L929-conditioned medium was obtained from L929 cells plated in a 10-cm dish containing 10 mL of L929 medium for 3 days to generate macrophage colony-stimulating factor. Primary bone marrow-derived macrophages (BMDMs) were obtained from bone marrow cells (BMCs), which were flushed from the bones of BALB/c mice and filtered through nylon mesh. BMCs were differentiated into macrophages in BMDM medium containing complete RPMI1640 medium, 20% L929-conditioned medium, 20% FBS, and 100 U/mL penicillin, and 100 μg/mL streptomycin. Cells were cultured in a 10 cm dish at a density of 3×10^5 cells/mL and maintained in 5% CO2, 37°C incubator. Six days after initial BMC cell culture, cell surface antigen F4/80 was detected by flow cytometry, the cellular differentiation reached a purity of about 90%. Stable overexpressing BMDMs-AIM2 cells were obtained by infection with pCDH–CMV-MCS-EF1-AIM2 lentivirus generated by HEK293T. The same amount of vector lentivirus was used as a control.

Coculture assay

In coculture assay with macrophages and tumor cells, Renca cells (4×10^5/well) were added in 6-well plates containing the 2 mL medium. Simultaneously, macrophages (BMDMs, BMDMs-Ctrl, or BMDM-AIM2) were seeded onto the inserts of 6-well Transwell (membrane pore size of 0.4 μm, Corning) at a density of 8×10^5 cells per insert with 2 ml of media. The inserts with the macrophages were then placed into the

Table 1
The used primers were presented.

	Forward primer	Reverse primer
GAPDH (human)	ATCCCATCACCATCTTCCAG	GAGTCCTTCCACGATACCAA
GAPDH (murine)	ACCACAGTCCATGCCATCAC	TCCACCACCCTGTTGCTGGTA
AIM2 (human)	GGCCCAGCAGGAATCTATCA	GCTTGCCTTCTTGGGTCTCA
AIM2 (murine)	AGTACCGGGAAATGCTGTTGTT	CCTATCTGCCACGTCGAGTGT
iNOS (murine)	GAGCTCGGGTTGAAGTGGTATG	GAAACTATGGAGCACAGCCACAT
CD206 (murine)	TTCAGCTATTGGACGCGAGG	GAATCTGACACCCAGCGGAA
Arg-1 (murine)	CTCCAAGCCAAAGTCCTTAGAG	AGGAGCTGTCATTAGGGACATC
IL-10 (murine)	GCTCTTACTGACTGGCATGAG	CGCAGCTCTAGGAGCATGTG
IL-12 (murine)	GGAAGCACGGCAGCAGAATA	AACTTGAGGGAGAAGTAGGAATGG
TNF-α (murine)	AAGCCTGTAGCCCACGTCGTA	GGCACCACTAGTTGGTTGTCTTTG

culture 6-well plate that contained the Renca cells. At different time points after coculture, macrophages from the cocultured system were collected for further experiment.

Real-time cell (RTCA) assay

The cell proliferation was determined using an xCELLigence RTCA SP instrument (ACEA Biosciences). Renca cell culture media (50 μL) was added to each well of 2×8-well E-Plates (ACEA Biosciences), and the background impedance was measured and displayed as the cell index. Then, cells (1×10^4/well) were seeded onto an E-Plate in a volume of 150 μL (100 μL Renca cell medium plus 50 μL culture supernatant of macrophages) and allowed to passively adhere to the electrode surface. The E-Plate was kept at an ambient temperature inside a laminar flow hood for 30 min and then transferred to the RTCAMP instrument inside a cell culture incubator. Data recording was initiated immediately at 15-min intervals for the entire duration of the experiment. Data acquisition was resumed to monitor the cells based on the viability of attached cells, as reflected by cell index values.

Colony formation assay

For the colony formation assay, macrophages were seeded at a density of 8×10^5 cells per insert of 6-well Transwell with 2 mL of media. Then Renca cells (1×10^3 cells/well) were seeded in a 6-well plate. Seven days after coculture, survival colonies were fixed with 4% paraformaldehyde for 10 min and stained with the crystal violet staining solution (Byotime Biotech) and counted under the microscope.

Cell apoptosis detection

Renca cells were collected from the coculture system and rinsed twice with PBS at 72 h post-treatment. Flow cytometry analysis of cell apoptosis was performed using an Annexin V-FITC/PI apoptosis detection kit (BD Biosciences) according to the manufacturer's instructions.

Cell migration assay

For the migration assay, 5×10^4 Renca cells suspended in 200 μL of serum-free medium were seeded on the upper compartment of 24-well Transwell culture chamber (membrane pore size of 8 μm), and 2×10^5 macrophages suspended in 600 μL of complete medium was added to the lower compartment. After 24 h incubation at 37°C, cells were fixed with methanol. Migrated cells on the lower side of the filter were stained with crystal violet and counted.

Caspase-1 activity detection

Caspase-1 colorimetric activity assay kit (Solarbio Biotech) was applied to detect caspase-1 activity according to the manufacturer's instructions. This assay was based on the ability of caspase-1 to change acetyl-Tyr-Val-Ala-Asp-p-nitroaniline (Ac-YVAD-pNA) into the yellow formazan product pNA. Briefly, the supernatant was collected from extracts and centrifuged at 12,000 g for 10 min, and detected protein concentration (1–3 $\mu g/\mu L$) by using the Bradford method. A volume of 10–35 μL of supernatant was incubated with 5 μL 2 mM Ac-YVAD-pNA substrate 2 h at 37 °C. Then, the absorbance values of pNA were read on a spectrophotometer at the optical density 405 nm (OD_{405}). The percentage of caspase-1 activity changes was calculated by the radio of OD_{405} of the experimental wells to that of the control wells.

Immunoblot analysis

Cells were harvested and resuspended in lysis buffer. The total protein concentration was determined with a bicinchoninic acid protein assay kit (Beyotime) according to the manufacturer's protocol. Protein samples were solubilized in sodium dodecyl sulfate (SDS) buffer by heating at 95°C for 10 min, and then separated on a 12% SDS polyacrylamide gel, transferred to polyvinylidene difluoride membranes. Membranes were blocked in 5% BSA solution and incubated with primary antibody against AIM2 (Cell Signaling Technology), ASC (Santa Cruz Biotechnology), Pro-Caspase-1 (Santa Cruz Biotechnology), Pro-IL-1β (Cell Signaling Technology), and GAPDH (Cell Signaling Technology) overnight at 4°C. Membranes were then washed with Tris-buffered saline containing 0.1% tween-20 (TBST), and were incubated with horseradish peroxidase linked secondary antibody (Cell Signaling Technology) for 2 h at room temperature and rinsed with TBST. Then the immunoreactive bands were detected by chemiluminescence using the ECL (Thermo Fisher Scientific). The density of the bands on the membrane were scanned and analyzed with an Image-J analyzer.

ELISA

The protein levels of IL-1β were measured by enzyme-linked immunosorbent assays (ELISA) in culture supernatant according to the manufacturer's instructions (eBioscience).

Flow cytometry analysis

For surface staining, cells were washed and incubated with FITC-anti-human CD14 (BioLegend), PE-anti-human CD197 (BioLegend), APC-anti-human CD206 (BioLegend), or PerCP-5.5-anti-mouse F4/80 (BioLegend), PE-anti-mouse CD11b (BioLegend), APC-anti-mouse CD206 (BioLegend) in PBS containing 2% FBS at 4°C for 30 min. Isotype-matched immunoglobulin served as controls. For intracellular staining, cells were fixed with fixation buffer (BD Biosciences) for 30 min at 4°C. The fixed cells were permeabilized with the permeabilization solution (BD Biosciences) at room temperature for 30 min. Cells were incubated overnight with Alexa Fluor 488-anti-mouse iNOS (eBioscience) at 4°C. Then, labeled cells were sorted by using the Aria III cell sorter (BD Biosciences) or analyzed by using BD FACSCanto II (BD Biosciences) with FACSDiva software.

Animal model and adoptive transfer

For the subcutaneous Renca tumor murine model, 5×10^5 Renca cells were subcutaneously inoculated into each mouse. BMDMs-Crtl or BMDMs-AIM2 (3×10^6 cells/mouse) were then intravenously injected into tumor models at day 1, 11, and 21 after the initial inoculation for a total of three times. Meanwhile, the inflammasome inhibitor Ac-YVAD-CMK (10 mg/kg, Sigma-Aldrich) was administrated intraperitoneally in treated mice. The survival status of tumor-bearing mice was monitored daily. Tumors were measured once every week. The tumor volume was calculated using the following formula: V (mm^3) = (length × $width^2$)/2. Animals were sacrificed, tumor tissues were surgically excised, and tumor weight was evaluated.

For the lung metastasis model, mice were intravenously injected with 1×10^6 Renca cells in the tail vein at day 0. Mice were adoptively transferred with BMDMs-Crtl or BMDMs-AIM2 (3×10^6 cells/mouse) at day 1, day 8, and day 15. The inflammasome inhibitor was also administrated intraperitoneally in treated mice. On day 21 after tumor inoculation, mice were sacrificed and lungs were removed, and the metastatic nodules were quantified.

Pathological analysis

For routine histological analysis, murine tissues were surgically resected and fixed in 4% paraformaldehyde (Sigma-Aldrich), embedded in paraffin and cut into 4 μm sections. H&E staining was performed according to the manufacturer's instructions, and the sections were assessed by a pathologist blinded to the treatment group. Pictures were acquired with a microscope (Nikon) equipped with photo software. Original magnification was × 100.

Statistical analysis

Statistical analysis was performed using the GraphPad Prism software. The mean values of data are presented as mean ± standard error of the mean (SEM). Comparison of two groups was analyzed using two-tailed Student's t-test. Multiple comparisons were performed using one-way ANOVA. The value was set as $^{*}p < 0.05$, $^{**}p < 0.01$, and $^{***}p < 0.001$ to represent statistical significance.

Results

AIM2 expression was negatively correlated with M2-like TAMs from renal cancer specimens

TAMs polarization is a critical regulator in tumor microenvironment and directly affects multiple steps of tumor development [31]. Therefore, polarization phenotypes of TAMs were determined in renal cancer specimens from human or mice. As shown in Fig. 1A and 1B, the percentages of $CD14^+$ TAMs were significantly increased in carcinoma tissues when compared with para-carcinoma tissues from human renal cancer specimens. Meanwhile, macrophage polarized phenotype was analyzed in TAMs. The results showed that the percentages of M2-like TAMs (expressing $CD14^+CD206^+$) were also higher than that of M1-like TAMs (expressing $CD14^+CD197^+$) in human carcinoma tissues (Fig. 1B). Similarly, the increased percentages of $CD11b^+F4/80^+$ TAMs were observed in carcinoma tissues from renal carcinoma models when compared with para-carcinoma tissues (Fig. 1C and 1D). The percentages of M2-like cells (expressing $CD11b^+F4/80^+CD206^+$) were higher than that of M1-like cells (expressing $CD11b^+F4/80^+iNOS^+$) in TAMs from murine tumor tissues (Fig. 1D). These results suggested that the TAMs infiltration and M2-like polarization were increased in renal carcinoma tissues.

To evaluate the correlation between AIM2 and TAMs polarization, we first detected the expression levels of AIM2 in TAMs from renal carcinoma specimens. In contrast to $CD14^+$TAMs from human para-carcinoma tissues, the expression levels of AIM2 were reduced in $CD14^+$TAMs from human carcinoma tissues (Fig. 1E). The reduced expression of AIM2 was also observed in $CD11b^+F4/80^+$TAMs from murine carcinoma tissues when compared with para-carcinoma tissues (Fig. 1F). Of note, the results of correlation analysis showed that AIM2 levels in $CD14^+$TAMs were negatively correlated with the percentages of $CD14^+$TAMs (Fig. 1G), and AIM2 expression in $CD11b^+F4/80^+$TAMs was also associated with the proportion of $CD11b^+F4/80^+$ TAMs (Fig. 1H). Moreover, AIM2 expression in TAMs also significantly correlated with the proportion of M2-like TAMs (Fig. 1I and 1J). These results indicate that the decreased AIM2 levels in TAMs were closely correlated with the infiltration percentage of different phenotype TAMs, particularly M2-like TAMs, implied that AIM2 expression might be involved in the regulation of TAMs polarization in tumor microenvironment.

Overexpression of AIM2 in macrophages reversed renal carcinoma cell-induced M2 phenotype transfer to M1

To investigate AIM2 function in TAMs polarization, the coculture assay with macrophages and Renca cells was performed to mimic the tumor microenvironment in vitro. The overexpression of AIM2 in BMDMs (BMDMs-AIM2) was performed by lentivirus infection. The western blot result showed that a significant upregulated expression of AIM2 in BMDMs-AIM2 compared with BMDMs-Ctrl (Fig. 2A and 2B). Moreover, the increased expression of inflammasome components (AIM2/Pro-caspase-1/Pro-IL-1β) was observed in BMDMs-AIM2 when compared with the control cells (Fig. 2A and 2B). Equally, caspase-1 activity and IL-1β production were significantly upregulated in BMDMs-AIM2 (Fig. 2C and 2D), which indicated that AIM2 inflammasome was formed and activated. Previous research has revealed that inflammasome activation is involved in M1 macrophage polarization in innate immune response [32]. Therefore, we detected the protein expression levels of iNOS and CD206 genes, which were related to macrophage polarization phenotype. Flow cytometry results showed a slight increased expression of iNOS and a significantly elevated expression of CD206 in BMDMs-Ctrl cocultured with Renca cells, but a significantly reduced expression of CD206 and a high expression of iNOS in BMDMs-AIM2 cocultured with Renca cells (Fig. 2E and 2F). Furthermore, the expression levels of macrophage polarization-related genes were detected by the real time PCR assay in macrophages from the coculture system. Compared with the BMDMs-Ctrl group, the BMDMs-AIM2 group showed that the mRNA levels of M2 phenotype markers (CD206, Arg-1, and IL-10) were significantly decreased, but M1 phenotype markers (iNOS, IL-12, and TNF-α) were increased (Fig. 2G). These results indicated the overexpression of AIM2 in macrophages enhanced inflammasome activation and reversed renal carcinoma cell-induced M2 phenotype transfer to M1.

AIM2-mediated M1 macrophages suppressed the malignant behaviors of renal carcinoma cells

To investigate the role of AIM2-mediated M1 macrophages in renal carcinoma cell growth, the cell proliferation and migration were investigated by the coculture assay with macrophages and Renca cells. The proliferation index by the RTCA assay was obviously reduced in Renca cells treated with the culture supernatant of BMDMs-AIM2 in contrast to BMDMs-Ctrl (Figs. 3A and 3B). Moreover, the colony formation assay also showed a decreased capability of colony formation of Renca cells cocultured with BMDMs-AIM2 (Figs. 3C and 3D). The apoptosis of Renca cells was increased in the BMDMs-AIM2 coculture group when compared with the BMDMs-Ctrl coculture group (Figs. 3E and 3F). Consistently, the reduced migration cells were seen by the Transwell assay in BMDMs-AIM2 cocultured group, implied that the migration ability of Renca cells was suppressed by AIM2-mediated macrophages (Figs. 4G and 4H). These results indicated that AIM2-mediated M1 macrophages could inhibit the malignant behaviors of renal cancer cells.

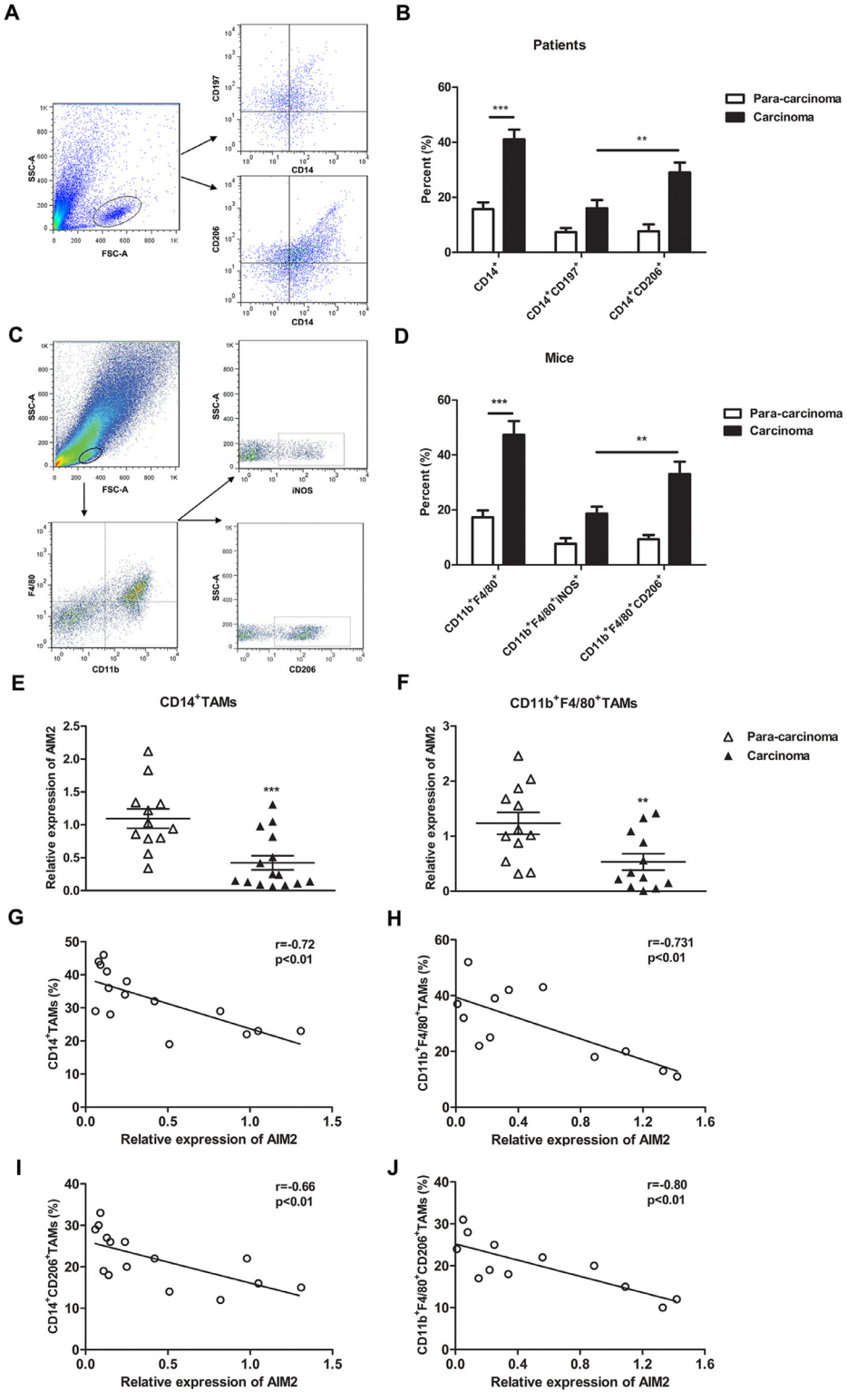

Fig. 1. AIM2 expression in TAMs was the association with M2-like phenotype in renal cancer. (A). Represents the flow cytometry analysis of $CD14^+CD197^+$TAMs or $CD14^+CD206^+$TAMs from human renal carcinoma tissues or para-carcinoma tissues. (B). The percentages of TAMs phenotype were evaluated in (A). (C). Represents the flow cytometry analysis of $F4/80^+CD11b^+iNOS^+$TAMs or $F4/80^+CD11b^+CD206^+$TAMs from carcinoma tissues or para-carcinoma tissues of Renca tumor models. (D). The percentages of TAMs phenotype were evaluated in (C). (E and F). AIM2 expression was detected by real time PCR in sorted TAMs from human (E) or murine (F) renal carcinoma tissues. (G). The correlation between the levels of AIM2 expression in $CD14^+$TAMs and the percent of $CD14^+$TAMs from human renal cancer specimens. Each symbol represents the data obtained from one patient, $n = 15$. (H). The association between AIM2 expression in $F4/80^+CD11b^+$TAMs and the percentages of $F4/80^+CD11b^+$TAMs from the murine model. Each symbol represents the data obtained from one mouse, $n = 12$. (I). The correlation between the levels of AIM2 expression in $CD14^+$TAMs and the percent of $CD14^+CD206^+$TAMs from human renal cancer specimens. (J). The association between AIM2 expression in $F4/80^+CD11b^+$TAMs and the percentages of $F4/80^+CD11b^+CD206^+$TAMs from murine model. Data are shown as means ± SD. The different significance levels were set at $^{**}p < 0.01$ and $^{***}p < 0.001$.

The inflammasome activation is required for AIM2-mediated M1 macrophages in the suppression of tumor malignant behaviors

It has now been shown that inflammasome is able to give the corresponding contribution of innate immune responses for the inhibition of tumor growth [33]. To validate whether AIM2-mediated M1 macrophages suppressed the growth of renal cancer cells by enhancing the inflammasome activation, the coculture assay with Renca cells and BMDMs-AIM2 followed with or without the downstream inflammatory caspase inhibitors YVAD-CMK. Compared with the control-treated group, the inhibitor-treated group showed the reduced levels of capspase-1 or IL-1β in cocultural supernatant (Figs. 4A and 4B), indicated that the inflammasome activation was blocked in BMDMs-AIM2. Furthermore, the decreased M1 phenotype and increased M2 pheno-

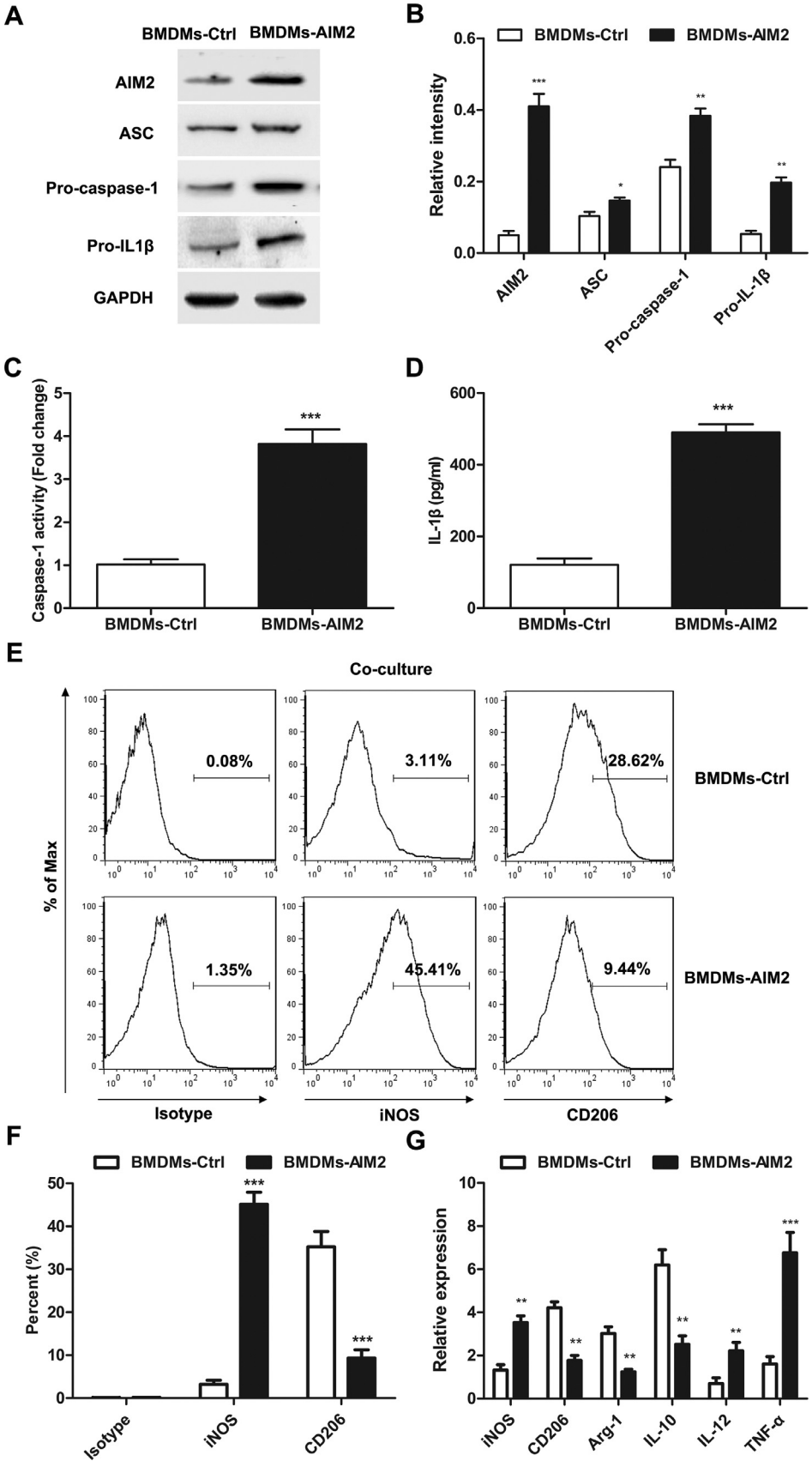

Fig. 2. Overexpression of AIM2 in macrophages reversed renal carcinoma cell-induced M2 phenotype transfer to M1. (A). The expression of AIM2 inflammasome components were measured by western blot in BMDMs infected with AIM2 lentivirus or control. (B). The relative expression of AIM2, ASC, Pro-caspase-1, or Pro-IL-1β relative to GAPDH in (A). (C). At 48 h after coculture of macrophages and renal carcinoma cells, the levels of caspase-1 were measured in the coculture supernatant. (D). IL-1β levels were detected by ELISA in the coculture supernatant. (E). Flow cytometry analyses were performed to assess percentages of expressing iNOS or CD206 on BMDMs-AIM2 or BMDMs-Ctrl from the cocultured system. (F). The percentages of M1 or M2 phenotype macrophages in (E). (G). At 24 h after coculture, the expression of iNOS, CD206, Arg-1, IL-10, IL-12, and TNF-α were determined by real time PCR in BMDMs-AIM2 or BMDMs-Ctrl. Data are representative of three experiments and presented as the means ± SD. The different significance levels were set at $^{*}p < 0.05$, $^{**}p < 0.01$, and $^{***}p < 0.001$; ns, not significant.

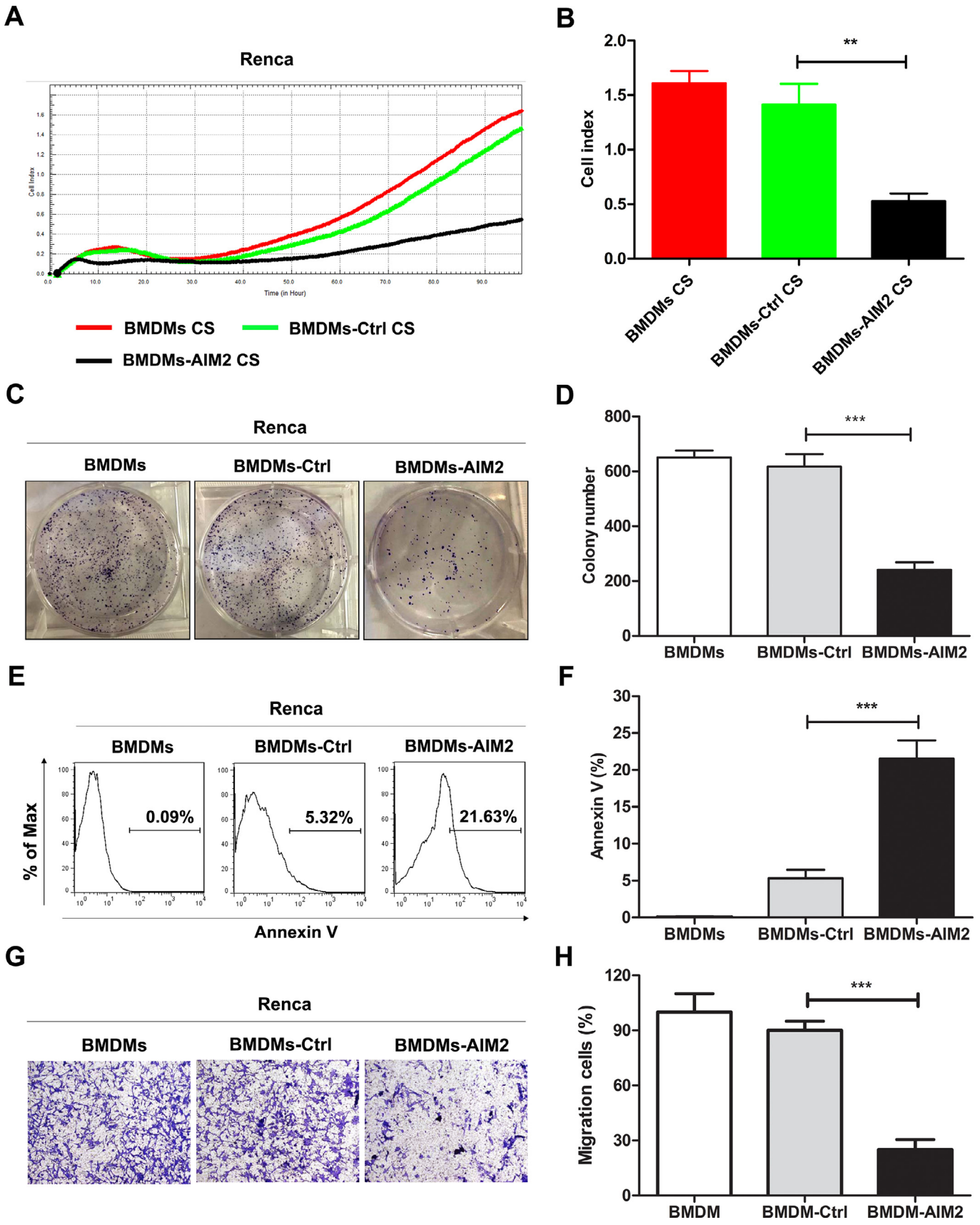

Fig. 3. AIM2-mediated M1 macrophages reduced the proliferation and migration of renal cancer cells. (A and B). Cell proliferation was determined by RTCA in Renca cells with or without the culture supernatant of BMDMs-AIM2 or BMDMs-Ctrl. (C and D). The colony formation capability was detected in Renca cells cocultured with BMDMs-AIM2 or BMDMs-Ctrl at day 7. (E). The apoptosis was detected by flow cytometry in Renca cells from the coculture system. (F). Statistical histograms of the percentage of apoptotic cells in (E), respectively. (G and H). Cell migration assay was performed in Renca cells from the coculture system. Data are representative of three experiments and presented as the means ± SD. The different significance levels were set at $^{**}p < 0.01$ and $^{***}p < 0.001$.

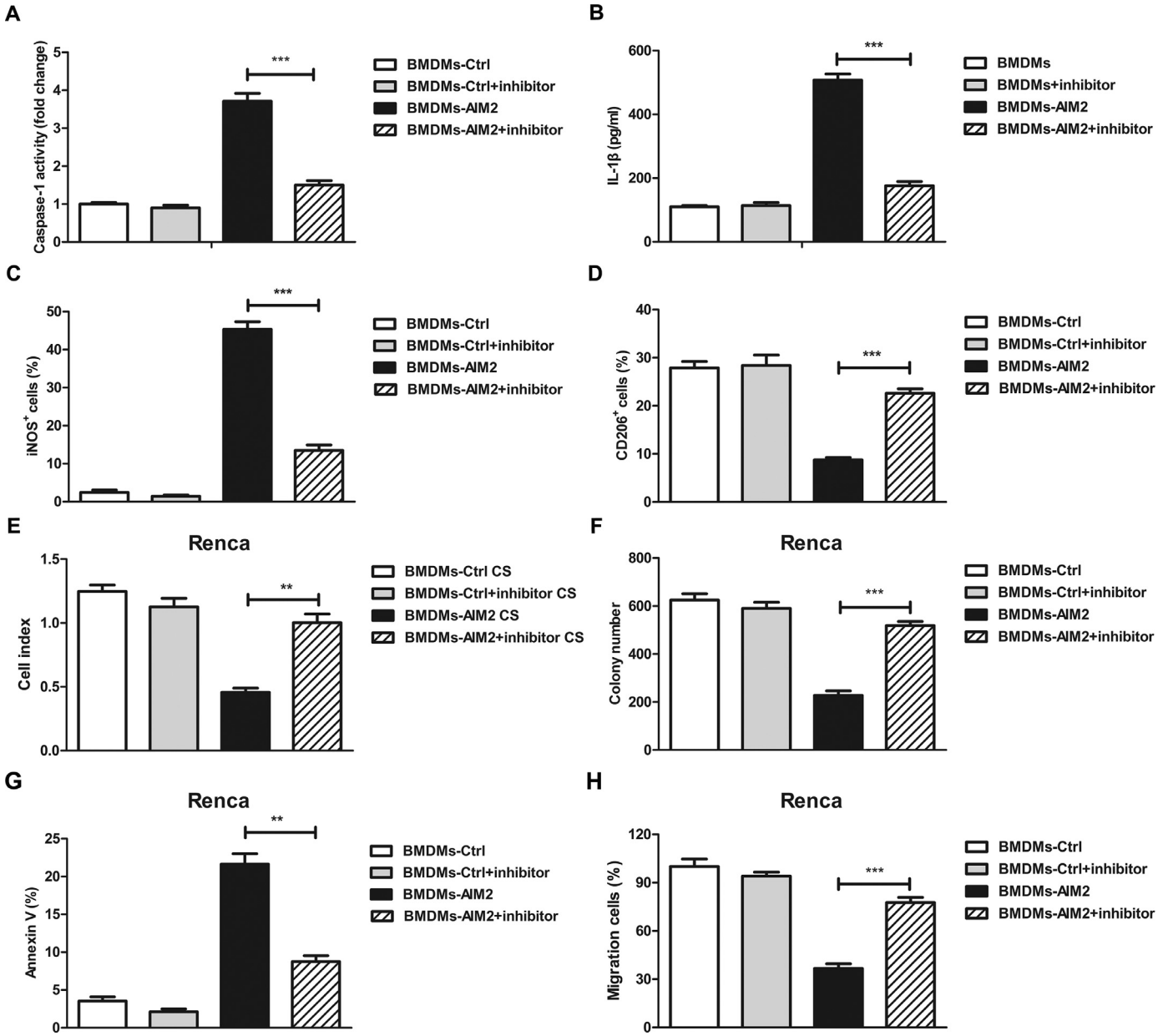

Fig. 4. AIM2-mediated M1 macrophages inhibited the growth of renal carcinoma cells through inflammasome activation. BMDMs-AIM2 or BMDMs-Ctrl was treated with or without Ac-YVAD-MCA (50 μmol/L) in the coculture assay. (A). 48 h after treatment, the levels of caspase-1 were measured in coculture supernatant. (B). IL-1β levels were detected by ELISA in coculture supernatant. (C and D). The percentages of iNOS$^+$ cells (C) or CD206$^+$ cells (D) were detected by flow cytometry in BMDMs-AIM2 or BMDMs-Ctrl from the cocultured system with or without inhibitor treatment. (E). The proliferation was detected by the RCTA assay in Renca cells with or without inhibitor-treated macrophage culture supernatant. (F). Clone formation of Renca cells was measured in the cocultured system with or without inhibitor treatment. (G). The apoptosis was detected by flow cytometry in Renca cells cocultured with inhibitor-treated macrophages. (H). The migration was measured in Renca cells cocultured with inhibitor-treated macrophages. Data are from one representative experiment of three performed and presented as the mean ±SD. The different significance levels were set at $^{**}p < 0.01$ and $^{***}p < 0.001$.

type were observed in BMDMs-AIM2 from inhibitor-treated the coculture group (Figs. 4C and 4D). Accordingly, the inhibition of Renca cell proliferation was prevented in the inhibitor-treated group (Figs. 4E and 4F). As showed in Fig. 4G, the apoptosis of Renca cells was also reduced in the inhibitor-treated group in contrast to the control-treated group. Furthermore, when compared with the control-treated group, the inhibitor-treated group showed decreased suppression of Renca cell migration (Fig. 4H). These data indicated that the inflammasome activation is required for AIM2-mediated M1 macrophages in the inhibition of malignant behaviors of renal cancer cells.

AIM2-mediated macrophages suppressed the subcutaneous tumor growth or lung metastasis in the renal carcinoma model

To further evaluate the therapeutic efficacy of AIM2-mediated M1 macrophages in vivo, mice bearing subcutaneous Renca tumor were injected intravenously with BMDMs-AIM2 or BMDM-Ctrl; meanwhile, the inflammasome inhibitor AC-YVAD-CMK was administrated intraperitoneally in treated mice. After tumor cell inoculation, tumor volumes were measured every week. As showed in Figs. 5A and 5B, tumor growth was significantly suppressed in the BMDM-AIM2-treated group when

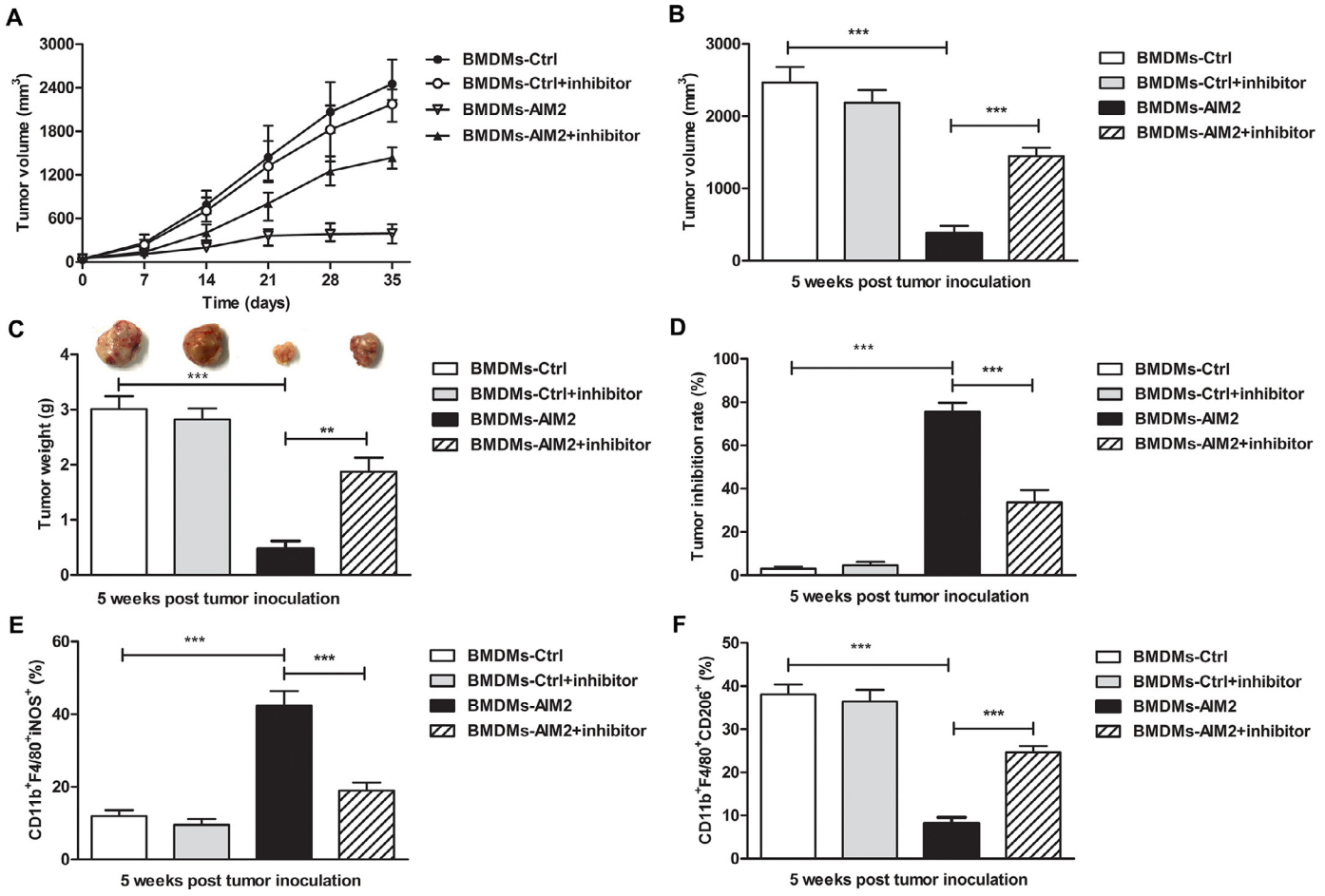

Fig. 5. The administration of BMDMs-AIM2 inhibits the tumor growth of subcutaneous Renca tumor mice. The subcutaneous Renca tumor mice were administrated intravenously BMDMs-Crtl or BMDMs-AIM2 (3×10^6 cells/mouse) at day 1, 11, and 21 after the initial inoculation for a total of three times. Meanwhile, the inflammasome inhibitor Ac-YVAD-CMK (10 mg/kg) was administered intraperitoneally in treated-mice. (A). Tumor progression of Renca tumor mice was evaluated by the measurement of tumor volume once per week from day 0 to day 35. (B). The tumor volumes were measured at week 5 after tumor inoculation. (C). The present images of tumor and tumor weights. (D). Tumor inhibition rate. (E and F). The frequencies of $CD11b^+F4/80^+iNOS^+$TAMs or $CD11b^+F4/80^+CD206^+$TAMs were analyzed in tumor tissues. The experiments were performed with 5 mice per group. Data shown are representative of three experiments. Data are means ± SD, $^{**}p<0.01$, and $^{***}p<0.001$.

compared with the control-treated group. Accordingly, the decreased weight of tumor and the increased inhibition rate of tumor were observed in the BMDM-AIM2-treated group (Figs. 5C and 5D). Moreover, the BMDM-AIM2-treated group showed the increased percentages of M1 TAMs (expressing $CD11b^+F4/80^+iNOS^+$) (Fig. 5E) and the reduced percentages of M2 TAMs (expressing $CD11b^+F4/80^+CD206^+$) (Fig. 5F) in tumor tissues. Meanwhile, we also found that the administration of inflammasome inhibitor reduced the anti-tumor activities of BMDMs-AIM2 accompanied with the decreased percentages of M1 TAMs in subcutaneous Renca tumor mice (Figs. 6A-6F), indicated that the anti-tumor effect of BMDMs-AIM2 depends on inflammasome activation-mediated M1 macrophages.

To assess whether BMDMs-AIM2 could also protect mice from tumor metastasis, lung metastasis models of renal carcinoma were established. The lung metastasis mice were intravenously injected with BMDMs-AIM2 followed with or without inflammasome activation inhibitor. At day 21 after tumor inoculation, mice were sacrificed and lungs were removed, and the visible metastases were counted. BMDMs-AIM2 treatment dramatically reduced the number of lung metastases when compared with BMDMs-Ctrl treatment, but the suppression of lung metastases was blocked by the inflammasome inhibitor (Figs. 6A and 6B). The protective efficacy of BMDMs-AIM2 was further confirmed by the H&E staining of lung tissues from the lung metastasis model (Fig. 6C). The analysis of the pathological section showed the decreased counts of lung metastases in the BMDMs-AIM2 group (Fig. 6D). M1-like or M2-like TAMs were analyzed by flow cytometry on day 21 after tumor inoculation. Increased tumor infiltrations of M1 TAMs were observed in BMDMs-AIM2-treated mice when compared with BMDMs-Ctrl-treated mice, while the increased percentages of M1 TAMs were suppressed by inhibitor treatment (Figs. 6E and 6F). These results indicated that the administration of BMDMs-AIM2 enhanced M1 TAMs infiltration and suppressed tumor lung metastasis of renal carcinoma. Taken together, these results indicated that AIM2 could enhance the macrophage polarization switch from M2 phenotype to M1 through inflammasome signaling and thus effectively prevent the aggravation of renal cancer (Fig. 7).

Discussion

Renal cancer is influenced by various factors in the development of pathological stages [34]. TAMs are considered more abundant tumor-infiltrating immune cells for fostering tumor progression [35]. Evidence shows that a switch in macrophage phenotype from M1 to M2 could influence the pathogenesis of tumor progression and metastasis [36,37]. Therefore, the concept was designed to repolarize TAMs from M2 to M1, which may be effective to treat RCC by using pro-inflammatory responses. In this study, our results showed that the overexpression of

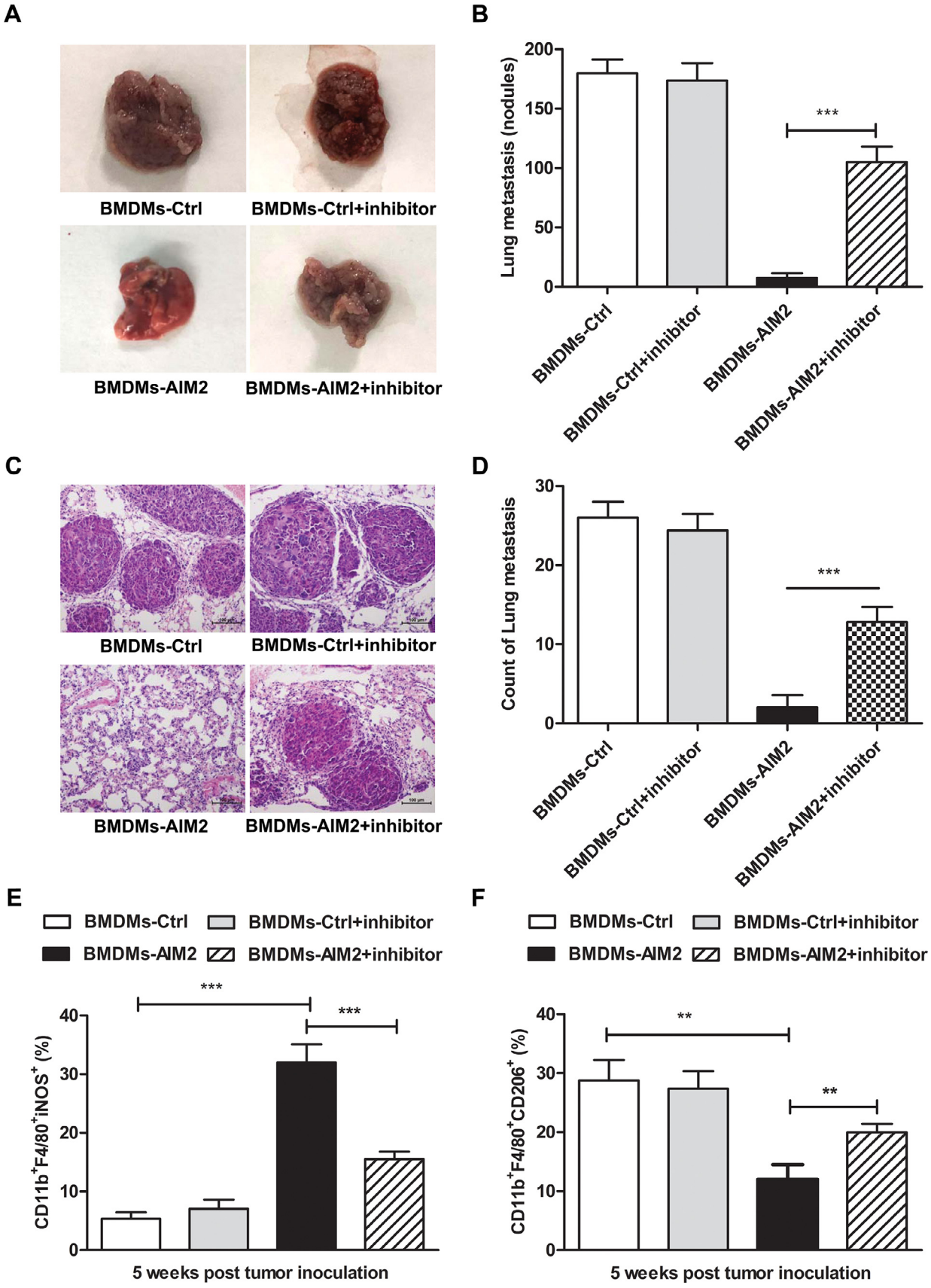

Fig. 6. Therapeutic effects of BMDMs-AIM2 in the lung metastasis model. (A). The present images of lung tumors excised from mice. (B). The numbers of metastatic nodules were quantified in the lungs of the tumor-bearing mice. (C). The present images of H&E staining for lung tissues. (D). Counts of lung metastasis were analyzed. (E and F). Mice were sacrificed on day 21 after tumor inoculation; frequencies of $CD11b^+F4/80^+iNOS^+$TAMs or $CD11b^+F4/80^+CD206^+$TAMs in lung tumor tissues. Each experiment was performed independently at least three times, and the results of one representative experiment are shown. Data, means ± SD, $^{**}p < 0.01$, and $^{***}p < 0.001$.

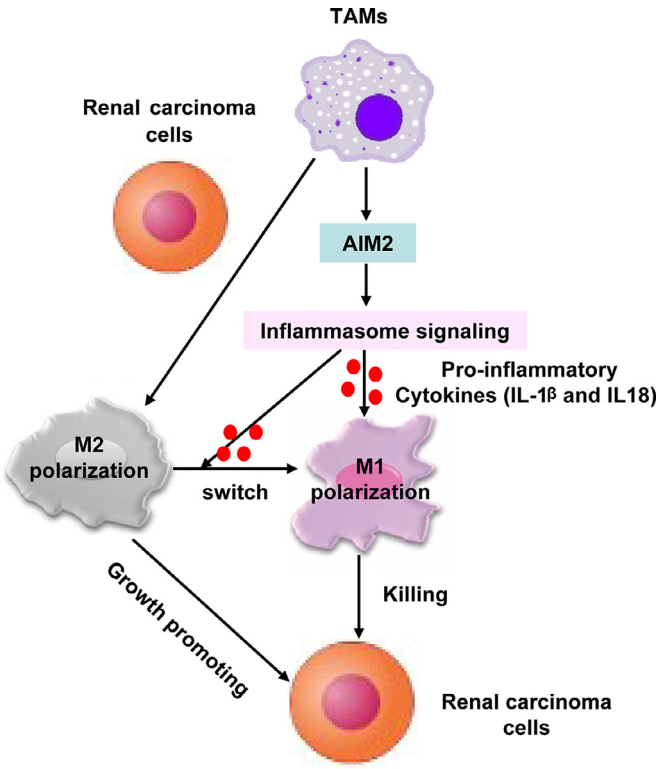

Fig. 7. Schematic illustration for AIM2-mediated M1 macrophages inhibited the growth of renal cancer cells. The overexpression of AIM2 in macrophages resulted in inflammasome signaling and promoted caspase-1 activation to produce the pro-inflammatory cytokine IL-1β. These cytokines then exert promoting effects on the switch from macrophage M2 polarization phenotype to M1. The increased M1 macrophages inhibited the growth of renal cancer cells.

AIM2 in macrophages could switch anti-inflammatory M2 phenotypic polarization induced by tumor cells to pro-inflammatory M1 through inflammasome activation, thus exerting an anti-tumor effect in renal carcinoma.

TAMs are presented in high density and different polarization in tumor microenvironment of solid tumors [38,39]. Our results showed that TAMs were significantly increased in human renal carcinoma tissues when compared with para-carcinoma tissues. Furthermore, the percentages of M2-like TAMs were higher than that of M1-like TAMs in carcinoma tissues. Similarly, the same results were observed in renal cancer models. To evaluate whether the AIM2 expression was associated with TAMs polarization, we detected the mRNA levels of AIM2 in TAMs from human or murine tumor tissues. AIM2 expression was reduced in TAMs from carcinoma tissues when compared with the TAMs from para-carcinoma tissues of human or murine specimens. TAMs predominantly exhibit an M2-like phenotype in malignant tumors. Of note, the correlation analysis results indicated that AIM2 expression was also negatively correlated with the proportion of M2-like phenotype TAMs. These results indicate that the changed AIM2 expression might be involved in the regulation of TAMs polarization in tumor microenvironment.

AIM2 function was not clearly understood in the differentiation of infiltrated TAMs from tumor microenvironment. To mimic tumor microenvironment, the coculture system of macrophages/Renca cell was established in vitro. The expression levels of M2 phenotype markers (CD206) were significantly decreased, but the levels of M1 phenotype markers (iNOS) were increased in BMDMs-AIM2 when compared with BMDMs-Ctrl from the coculture assay. Real-time PCR results also demonstrated that M2 phenotype markers (CD206, Arg-1, or IL-10) were downregulated, M1 phenotype markers (iNOS, IL-12, or TNF-α) were upregulated in BMDMs-AIM2 in contrast to BMDMs-Ctrl from the coculture system. These results indicated that the overexpression of AIM2 in macrophages could reverse Renca cell-induced M2 phenotype transfer to M1.

The inflammasome responds to multiple danger signals, including a decrease in cytosolic potassium concentrations and an increase in cytosolic DNA levels, dying tumor cells and bacterial products [40]. M1 macrophages mediated by AIM2 might contribute to the stimulation of the inflammasome activation by recognizing dsDNA from dying tumor cells. The activation of inflammasome has been reported to inhibit cancer cell invasion and metastasis, angiogenesis, or tumorigenesis in model systems, which suggests that the defense of inflammasome in tumor cells is a tumor-suppression mechanism [20,41]. Our data demonstrated that the overexpression of AIM2 in macrophages significantly enhanced the expression of inflammasome competence (AIM2/Pro-caspase-1/Pro-IL-1β). Equally, caspase-1 activity and IL-1β production were significantly upregulated in overexpressing AIM2 macrophages, which indicated that AIM2 inflammasome was formed and activated. It is well known that tumor cell proliferation, migration, and invasion are main processes of metastasis, which remains the major cause of mortality in patients with renal cancer. AIM2-mediated M1 macrophages could suppress the proliferation and migration of renal carcinoma cells by enhancing the inflammasome activation in the cocultured system. These data indicated that the inhibition of malignant behaviors of renal carcinoma cells by AIM2-mediated M1 macrophages was mainly dependent on the inflammasome activation.

We further evaluate the therapeutic efficacy of AIM2-mediated M1 macrophages in subcutaneous Renca tumor models. The volume and weight of tumor was decreased in BMDM-AIM2-treated group. Moreover, the increased percentages of M1 TAMs and the reduced percentages of M2 TAMs were observed in BMDM-AIM2-treated group. Meanwhile, we also observed that the administration of inflammasome inhibitor reduced the anti-tumor activities of BMDMs-AIM2 in Renca tumor mice, which indicated that the anti-tumor effect of AIM2-mediated BMDMs depended on inflammasome activation. In the lung metastasis model of renal carcinoma, BMDMs-AIM2 treatment dramatically reduced the number of lung metastases, but the reduction of lung metastases caused a blockade in the inhibitor-treated BMDMs-AIM2 group. The increased infiltration of M1 TAMs and reduced infiltration of M2 TAMs were observed in mice treated with the BMDMs-AIM2 group when compared with the control group. These results indicated that BMDMs-AIM2 enhances M1 TAMs infiltration and suppresses tumor lung metastasis of renal carcinoma. Taken together, these data indicated that BMDMs-AIM2 treatment could effectively prevent the aggravation of tumor. Changing the polarized phenotype of macrophages is able to limit TAMs immunosuppression, which seems to be a promising approach to treat cancer. For recurrent tumor immunotherapy, targeted therapy of TAMs might be needed to combine with other therapies (such as immunocheckpoint inhibitors), which is required to further study in future.

Conclusion

In conclusion, our results suggested that AIM2-mediated M1 macrophages could inhibit malignancies of renal cancer by switching the phenotype from anti-inflammatory M2 to pro-inflammatory M1 through the enhancement of the inflammasome pathway. Our results provide a possible molecular mechanism responsible for the modulation of TAMs polarization in the tumor microenvironment of renal carcinoma and open a new potential therapeutic approach for renal carcinoma.

Author contributions

Conceived and designed the project: DC, JZ; Performed the project: DC, ZC, DQ, SYS, NJ; Analysed the data: DC, ZC, DQ SYS, NJ; Contributed reagents/materials/analysis tools: CZ GW, LF, HL, HT, HL, JZ; Wrote the paper: DC, ZC. All authors read and approved the final manuscript.

Declaration of Competing Interests

The authors declare that they have no competing interests.

Acknowledgments

This project is supported by grants from the National Natural Science Foundation of China (Nos. 82072814, 81702499, and 81871869), Jiangsu Province Natural Science Foundation (No. BK20170266), Natural Science Fund for Colleges and Universities in Jiangsu Province (No. 19KJB310001), Jiangsu Provincial Key Medical Discipline, The Project of Invigorating Health Care through Science, Technology, and Education (No. ZDXKA2016014).

References

[1] A. Znaor, J. Lortet-Tieulent, M. Laversanne, A. Jemal, F. Bray, International variations and trends in renal cell carcinoma incidence and mortality, Eur. Urol. 67 (2015) 519–530.
[2] H.T. Cohen, F.J. McGovern, Renal-cell carcinoma, N. Engl. J. Med. 353 (2005) 2477–2490.
[3] J.J. Hsieh, M.P. Purdue, S. Signoretti, C. Swanton, L. Albiges, M. Schmidinger, et al., Renal cell carcinoma, Nat. Rev. Dis. Primers 3 (2017) 1–42.
[4] R.L. Siegel, K.D. Miller, A. Jemal, Cancer statistics, 2018, CA Cancer J. Clin. 68 (2018) 7–30.
[5] U. Capitanio, K. Bensalah, A. Bex, S.A. Boorjian, F. Bray, J. Coleman, et al., Epidemiology of renal cell carcinoma, Eur. Urol. 75 (2019) 74–84.
[6] B. Ljungberg, S.C. Campbell, H.Y. Choi, D. Jacqmin, J.E. Lee, S. Weikert, et al., The epidemiology of renal cell carcinoma, Eur. Urol. 60 (2011) 615–621.
[7] L. Cerbone, C. Cattrini, G. Vallome, M.M. Latocca, F. Boccardo, E. Zanardi, Combination therapy in metastatic renal cell carcinoma: back to the future? Semin. Oncol. 47 (2020) 361–366.
[8] I. Richter, J. Dvorak, Treatment of metastatic renal cell carcinoma, Klin. Onkol. 31 (2018) 110–116.
[9] L.M.A. Aparicio, I.P. Fernandez, J. Cassinello, Tyrosine kinase inhibitors reprogramming immunity in renal cell carcinoma: rethinking cancer immunotherapy, Clin. Transl. Oncol. 19 (2017) 1175–1182.
[10] W. Hu, X. Li, C. Zhang, Y. Yang, J. Jiang, C. Wu, Tumor-associated macrophages in cancers, Clin. Transl. Oncol. 18 (2016) 251–258.
[11] A. Salmaninejad, S.F. Valilou, A. Soltani, S. Ahmadi, Y.J. Abarghan, R.J. Rosengren, et al., Tumor-associated macrophages: role in cancer development and therapeutic implications, Cell Oncol. (Dordr) 42 (2019) 591–608.
[12] F.O. Martinez, A. Sica, A. Mantovani, M. Locati, Macrophage activation and polarization, Front. Biosci. 13 (2008) 453–461.
[13] B. Ruffell, N.I. Affara, L.M. Coussens, Differential macrophage programming in the tumor microenvironment, Trends Immunol. 33 (2012) 119–126.
[14] M. Genin, F. Clement, A. Fattaccioli, M. Raes, C. Michiels, M1 and M2 macrophages derived from THP-1 cells differentially modulate the response of cancer cells to etoposide, BMC Cancer 15 (2015) 1–14.
[15] A. Mantovani, S. Sozzani, M. Locati, P. Allavena, A. Sica, Macrophage polarization: tumor-associated macrophages as a paradigm for polarized M2 mononuclear phagocytes, Trends Immunol. 23 (2002) 549–555.
[16] R. Noy, J.W. Pollard, Tumor-associated macrophages: from mechanisms to therapy, Immunity 41 (2014) 49–61.
[17] J. Lugrin, F. Martinon, The AIM2 inflammasome: sensor of pathogens and cellular perturbations, Immunol. Rev. 281 (2018) 99–114.
[18] K. Schroder, D.A. Muruve, J. Tschopp, Innate immunity: cytoplasmic DNA sensing by the AIM2 inflammasome, Curr. Biol. 19 (2009) R262–R265.
[19] V. Hornung, A. Ablasser, M. Charrel-Dennis, F. Bauernfeind, G. Horvath, D.R. Caffrey, et al., AIM2 recognizes cytosolic dsDNA and forms a caspase-1-activating inflammasome with ASC, Nature 458 (2009) 514–518.
[20] R. Karki, S.M. Man, T.D. Kanneganti, Inflammasomes and Cancer, Cancer Immunol. Res. 5 (2017) 94–99.
[21] S.M. Man, R. Karki, T.D. Kanneganti, AIM2 inflammasome in infection, cancer, and autoimmunity: role in DNA sensing, inflammation, and innate immunity, Eur. J. Immunol. 46 (2016) 269–280.
[22] W. Zhang, Y. Cai, W. Xu, Z. Yin, X. Gao, S. Xiong, AIM2 facilitates the apoptotic DNA-induced systemic lupus erythematosus via arbitrating macrophage functional maturation, J. Clin. Immunol. 33 (2013) 925–937.
[23] D.P. Sester, V. Sagulenko, S.J. Thygesen, J.A. Cridland, Y.S. Loi, S.O. Cridland, et al., Deficient NLRP3 and AIM2 inflammasome function in autoimmune NZB mice, J. Immunol. 195 (2015) 1233–1241.
[24] S.J. Thygesen, K.E. Takizawa, A.A.B. Robertson, D.P. Sester, K.J. Stacey, Compromised NLRP3 and AIM2 inflammasome function in autoimmune NZB/W F1 mouse macrophages, Immunol. Cell Biol. 97 (2019) 17–28.
[25] D. Choubey, Absent in melanoma 2 proteins in the development of cancer, Cell. Mol. Life Sci. 73 (2016) 4383–4395.
[26] D. Chai, H. Shan, G. Wang, H. Li, L. Fang, J. Song, et al., AIM2 is a potential therapeutic target in human renal carcinoma and suppresses its invasion and metastasis via enhancing autophagy induction, Exp. Cell Res. 370 (2018) 561–570.
[27] I.F. Chen, F. Ou-Yang, J.Y. Hung, J.C. Liu, H. Wang, S.C. Wang, et al., AIM2 suppresses human breast cancer cell proliferation in vitro and mammary tumor growth in a mouse model, Mol. Cancer Ther. 5 (2006) 1–7.
[28] S. Dihlmann, S. Tao, F. Echterdiek, E. Herpel, L. Jansen, J. Chang-Claude, et al., Lack of Absent in Melanoma 2 (AIM2) expression in tumor cells is closely associated with poor survival in colorectal cancer patients, Int. J. Cancer 135 (2014) 2387–2396.
[29] L. Ponomareva, H. Liu, X. Duan, E. Dickerson, H. Shen, R. Panchanathan, et al., AIM2, an IFN-inducible cytosolic DNA sensor, in the development of benign prostate hyperplasia and prostate cancer, Mol. Cancer Res. 11 (2013) 1193–1202.
[30] B.R. Sharma, R. Karki, T.D. Kanneganti, Role of AIM2 inflammasome in inflammatory diseases, cancer and infection, Eur. J. Immunol. 49 (2019) 1998–2011.
[31] P. Pathria, T.L. Louis, J.A. Varner, Targeting tumor-associated macrophages in cancer, Trends Immunol. 40 (2019) 310–327.
[32] L.R. Lin, W. Liu, X.Z. Zhu, Y.Y. Chen, Z.X. Gao, K. Gao, et al., Treponema pallidum promotes macrophage polarization and activates the NLRP3 inflammasome pathway to induce interleukin-1beta production, BMC Immunol. 19 (2018) 1–9.
[33] J.E. Wilson, A.S. Petrucelli, L. Chen, A.A. Koblansky, A.D. Truax, Y. Oyama, et al., Inflammasome-independent role of AIM2 in suppressing colon tumorigenesis via DNA-PK and Akt, Nat. Med. 21 (2015) 906–913.
[34] X. Peng, J. Chen, J. Wang, S. Peng, S. Liu, K. Ma, et al., Natural history of renal tumours in von Hippel-Lindau disease: a large retrospective study of Chinese patients, J. Med. Genet. 56 (2019) 380–387.
[35] S. Zhang, E. Zhang, J. Long, Z. Hu, J. Peng, L. Liu, et al., Immune infiltration in renal cell carcinoma, Cancer Sci. 110 (2019) 1564–1572.
[36] P. Dhupkar, N. Gordon, J. Stewart, E.S. Kleinerman, Anti-PD-1 therapy redirects macrophages from an M2 to an M1 phenotype inducing regression of OS lung metastases, Cancer Med. 7 (2018) 2654–2664.
[37] Y. Wang, Y.X. Lin, S.L. Qiao, H.W. An, Y. Ma, Z.Y. Qiao, et al., Polymeric nanoparticles promote macrophage reversal from M2 to M1 phenotypes in the tumor microenvironment, Biomaterials 112 (2017) 153–163.
[38] T. Chanmee, P. Ontong, K. Konno, N. Itano, Tumor-associated macrophages as major players in the tumor microenvironment, Cancers (Basel) 6 (2014) 1670–1690.
[39] K.Y. Jung, S.W. Cho, Y.A. Kim, D. Kim, B.C. Oh, D.J. Park, et al., Cancers with higher density of tumor-associated macrophages were associated with poor survival rates, J. Pathol. Transl. Med. 49 (2015) 318–324.
[40] V. Petrilli, C. Dostert, D.A. Muruve, J. Tschopp, The inflammasome: a danger sensing complex triggering innate immunity, Curr. Opin. Immunol. 19 (2007) 615–622.
[41] D. Chai, N. Liu, H. Li, G. Wang, J. Song, L. Fang, et al., H1/pAIM2 nanoparticles exert anti-tumour effects that is associated with the inflammasome activation in renal carcinoma, J. Cell. Mol. Med. 22 (2018) 5670–5681.